



Immobilization of AgCl@TiO₂ on the woven wire mesh: Sunlight-responsive environmental photocatalyst with high durability

Hossein Azizi-Toupkanloo (PhD)^{a,*}, Mahdi Karimi-Nazarabad (PhD)^{b,c,*}, Gholam-Reza Amini^a, Abolfazl Darroudi (PhD)^c

^a Department of Chemistry, University of Neyshabur, Neyshabur 9319774446, Iran

^b Department of Chemistry, Faculty of Science, Ferdowsi University of Mashhad, Mashhad 9177948974, Iran

^c Department of Chemistry, Faculty of SamenHojaj, Mashhad Branch, Technical and Vocational University, Tehran, Iran

ARTICLE INFO

Keywords:

AgCl@TiO₂ thin film
Electrophoretic deposition
Woven wire mesh
Methamphetamine
Photocatalytic degradation
Photoelectrochemical

ABSTRACT

The immobilized AgCl@TiO₂ photocatalytic thin films were fabricated via electrophoretic deposition method. Affordability, scalability, and high chemical stability are some valuable characteristics making woven stainless steel wire mesh a suitable substrate for fabrication of photocatalyst film. The photocatalytic degradation efficiency of the thin film was investigated by removing hard-degradable methamphetamine under natural solar light. The AgCl@TiO₂ photocatalyst with AgCl content of about 5% showed the most photocatalytic degradation efficiency. Using Mott-Schottky plots, the flat band potential of prepared photocatalysts was estimated. The flat band potential showed that the conduction band of AgCl@TiO₂ is a better candidate for production of superoxide radicals than TiO₂. A film thickness of 1629 nm yields optimal photodegradation efficiency. A series of ten sequential cycles for photodegradation of methamphetamine was conducted using thin film which caused neither significant destruction on photocatalytic substrate nor any considerable reduction in efficiency whatsoever. The AgCl@TiO₂ thin film-induced mineralization of methamphetamine was reported to be approximately around 91 percent. The photoelectrochemical performance of TiO₂ and AgCl@TiO₂ thin film was evaluated by LSV technique under solar light and results show that after incorporation of AgCl, the photocurrent density corresponding to the oxygen evolution reaction significantly increased to 1.8 mA cm⁻² at 1.23 V vs RHE.

1. Introduction

The photocatalysis technique is an effectual method for degrading organic pollutants under the mild conditions due to its abundance, non-pollution, and cleanliness (Hao et al., 2018). Most of the experimental studies have been conducted on systems in which colloidal dispersion of photocatalyst are irradiated, while catalysts will likely need to be immobilized on fixed support materials (Adamek et al., 2019). The advantages of substituting colloidal dispersion with photocatalytic films can be summarized as: low cost, low particle aggregation, simple usage, high photodegradation efficiency, better light penetration in the absence of turbidity, thereby eliminating the need for photocatalytic regeneration and recovery, and effective pathways for electron transmission (Carbonaro et al., 2013).

In order to obtain broad-spectrum light-active photocatalysts, TiO₂ has been tested as a basic material by many researchers (Anitha et al., 2015; Elkoro et al., 2019; Monga et al., 2017; Tayebi et al., 2019). The

improvement of stabilizations of the photo-generated charge carrier is a crucial issue for light-harvesting systems in both photocatalytic and photovoltaic solar cells (Ganeshraja et al., 2018). Therefore, in order for solar light energy to be optimally harvested, many researchers fabricated modified TiO₂ via doping and compositing visible-light-active semiconductor nanoparticles on TiO₂ nanostructures. The intrinsic band structure of TiO₂ can be remarkably affected by incorporation of hetero-atoms into the crystal structure which, in turn, will broaden the photo-absorption light region. Based on different doping elements, TiO₂ doping with metals (cations) or nonmetal (anion) elements has been broadly applied (Brindha and Sivakumar, 2017; Chang et al., 2016; Hong et al., 2019; Yuan et al., 2017). More importantly, doping can enhance photocatalytic activity through separation of photo-induced electrons and holes. Silver halides due to some superior properties such as their good visible light absorption ability (Lv et al., 2018), photosensitivity property (Putri et al., 2016) (which attributable to their ionic point defects and the electron trapping (Wang et al., 2008) of these

* Corresponding authors at: Department of Chemistry, Faculty of Science, Ferdowsi University of Mashhad, Mashhad 9177948974, Iran (M. Karimi-Nazarabad). Department of Chemistry, University of Neyshabur, Neyshabur 9319774446, Iran (H. Azizi-Toupkanloo).

E-mail addresses: h.azizi@neyshabur.ac.ir (H. Azizi-Toupkanloo), m.kariminazarabad@gmail.com, mahdi_karimi@um.ac.ir (M. Karimi-Nazarabad).

<https://doi.org/10.1016/j.solener.2019.12.046>

Received 25 September 2019; Received in revised form 27 November 2019; Accepted 16 December 2019

0038-092X/ © 2020 International Solar Energy Society. Published by Elsevier Ltd. All rights reserved.

compounds leading to improvement of this property) are a suitable candidate for doping in TiO₂. For example, the improved photocatalytic activity of AgCl/TiO₂ photocatalysts in comparison to pure TiO₂ was reported by Huo and coworkers (Huo et al., 2010). They described the high efficiency prepared novel visible light-driven AgCl/TiO₂ photocatalyst to enhance Rhodamine B photodegradation activity. They suggested that in the presence of AgCl, the photodegradation efficiency of Rhodamine B could be increased to 94.96% under visible light. Recently, Yang and coworkers (Yang et al., 2018) demonstrated that the photocatalytic activity of Ag/AgCl/TiO₂ under irradiation for Rhodamine B has a significant enhancement compared to TiO₂ and Ag/TiO₂ photocatalysts.

A newly known class of environmental pollutants that are gaining considerable attention due to their environmental impacts and toxicological properties over the last decade are Pharmaceuticals products (Azizi-Toupkanloo et al., 2019; Jones et al., 2002; Kates et al., 2014; Ternes, 2001). Among the pharmaceutical pollutants, amphetamine-type stimulants such as methamphetamine are among most widespread pharmaceutical pollutants which are commonly abused as drugs; these pollutants can easily transmit through environmental aqueous media and be continuously consumed in an uncontrollable manner. Ongoing investigations have shown that these drugs can infiltrate and remain in aquatic environments (Kasprzyk-Hordern et al., 2009). For instance, Boleda and coworkers (Rosa Boleda et al., 2011) reported that drinking water in river Taff Italsy and Lambro River, Spain, have been concentrations of 3.22 and 2.1 ng L⁻¹ of methamphetamine, respectively. Therefore, the existence of psychoactive drugs such as methamphetamine in potable water can be considered as a life threatening problem. The removal efficiency for these pollutants is low and they may remain in treated wastewater even at low concentrations (Castiglioni et al., 2011; Evgenidou et al., 2015). There are a few researches performed on the degradation (Kuo et al., 2015) and biodegradation (Bagnall et al., 2013; Wang et al., 2018) of methamphetamine using nanomaterials. For example, Lin and coworkers (Lin et al., 2013) studied the photodegradation of methamphetamine using irradiated TiO₂ nanomaterial. It was found that, the UV-TiO₂ system was most significant, receiving 99.9% elimination of methamphetamine. Also, Kuo and coworkers (Kuo et al., 2015) evaluated the feasibility of removing methamphetamine by UV-illuminated TiO₂. They almost completely mineralized the methamphetamine from 10 mg L⁻¹ aqueous in 180 min with 0.1 g L⁻¹ of TiO₂ at pH 5. The sustainability of these materials in drinking water or wastewater, and also their non-removal by conventional methods, indicates the notability of photocatalysis as a possible technique for degradation of these materials.

The present study has three distinct features compared to other works: First, it uses an immobilized system for heterogeneous photocatalytic degradation of a pollutant, which facilitates its application to the semi-invasive scale photodegradation process. Second, an appropriate method, electrophoretic deposition, is used to deposit the photocatalyst on a suitable substrate, woven stainless steel wire mesh, with high durability. Third, in this work methamphetamine was selected as a hard-degradable contaminant which no reported for degradation with this photocatalyst. Also, the number of articles on AgCl doped TiO₂ as photocatalyst is limited. Various parameters such as film thickness, content percentage of AgCl in TiO₂ structure, pH, and concentration of methamphetamine were evaluated.

2. Experimental section

2.1. Chemicals

All chemicals including cetyltrimethylammonium bromide (CTAB, 99.0%, BDH), titanium isopropoxide (TTIP, 97.0%, Merck), ethylene glycol (EG, 99.8%, Merck), hydrochloric acid (37.0%, Merck), silver nitrate (99.0%, Merck), hydrochloric acid (37.0%, Merck), sodium hydroxide (≥97.00%, Fluka), methamphetamine hydrochloride

(Merck), and ethanol (99.9%, Bidestan) were analytical graded and used as received and no further purification was conducted.

2.2. Preparation of AgCl@TiO₂ and AgCl

Hydrothermal method was used to prepare AgCl@TiO₂ photocatalysts. This procedure includes addition of 1.2 mL TTIP into 10 mL of HCl solution under stirring followed by adding 50 mL of EG (Bottle A). A specific amount of AgNO₃ was dissolved in 5 mL distilled water and then, 1 g CTAB was dissolved in the solution (Bottle B) and stirred for 30 min. Solution Bottle B was added into solution A and stirred powerfully for 1 h. Following this, this dispersion was transferred to an autoclave and exposed to 150 °C heat for 20 h. The autoclave was normally cooled down to ambient temperature. The fabricated AgCl@TiO₂ nanomaterials were centrifuged and washed with ethanol and distilled water several times; a vacuum oven was used to dry the sample at 80 °C overnight. The AgCl@TiO₂ nanomaterials were prepared with the AgNO₃ contents of 0.005, 0.01, 0.03, and 0.05 g, denoted as 1-AgCl@TiO₂, 3-AgCl@TiO₂, 5-AgCl@TiO₂, and 7-AgCl@TiO₂, respectively. The pure TiO₂ nanoparticles (NPs) were prepared via similar procedure with the exception that AgNO₃ was not added. For preparation of AgCl nanoparticles, 2 mmol AgNO₃ dissolved in 30 mL of deionized water followed by the addition of 4 mL HCl (1 mol L⁻¹) under stirring for 30 min to form a clear solution. After, 30 mL deionized water was added under stirring for 45 min, the solution was placed in a 100 mL teflon lined stainless autoclave and heated to 150 °C and maintained for 20 h. The prepared powder was collected, washed several times with distilled water and dried at 80 °C for 12 h. The dried sample was calcined at 350 °C for 5 h in a muffle furnace.

2.3. Photocatalysis substrates fabrication

The prepared TiO₂ and AgCl@TiO₂ nanomaterials were amassed on a smoothed commercial stainless steel mesh substrates with dimensions of 2 × 2 cm² through electrophoretic deposition (EPD). The EPD is a reproducible, efficient, and simple method for the preparation of thin film.

In order to polish the substrate, oxalic and sulfuric acids were used as electrolyte mixture with emerge paper (grid from 200 to 1500), and then the sample was drowned in ethanol and acetone for 15 min under ultrasonic bath (BRANSON, 40 kHz), respectively. After 20 min of dispersing 0.02 g prepared nanomaterials in 25 mL acetone under ultrasonic bath, the EPD procedure of the photocatalyst thin film on woven stainless steel wire mesh substrates were performed. Then, 0.01 g of iodine was added to the prepared stabilized dispersion. This dispersion was utilized for EPD. During EPD procedure, a platinum plate was used as the counter electrode which separated from the working electrode by a distance of 10 mm in the electrophoretic cell. EPD was accomplished under potentiostatic modes using DC power supply (TF 102, TERCO) at a bias voltage of 20 V for a specific time. The obtained thin film was annealed in air at 450 °C for half an hour.

2.4. Photocatalytic experiments

The photocatalytic degradation of methamphetamine was performed under solar simulator light and natural solar light irradiation during sunny days in summer 2018 between 11 am and 2 pm (N = 36°15'6.682", E = 58°47'; 42.806" GPS coordinates). In a typical photocatalytic experiment, the fabricated substrates were immersed in an aqueous solution of 30 mL methamphetamine followed by magnetic stirring. The photocatalytic degradation setup was placed under direct natural solar light. The experimental conditions such as time, concentrations of the methamphetamine (6–40 mg L⁻¹), initial pH (3–11), AgCl% in photocatalyst, and the thickness of electrodeposited photocatalyst film was varied according to different setups. The degradation amount was measured according the λ_{max} of methamphetamine (at

208 nm), by UV–vis spectrophotometer. The equation given below can be used to obtain the catalytic degradation efficiency (CDE) of methamphetamine:

$$CDE\% = \frac{C_0 - C_t}{C_0} \times 100 \quad (1)$$

In this equation, C_0 and C_t are the initial concentration and the concentration of methamphetamine at time t , respectively. It is noteworthy that at least three repetitions was used for each measurement and the mean value was used in the graphs and the error amount in each case was represented by error bars.

The linear sweep voltammetry (LSV) experiments were performed for the photoelectrochemical studies. A conventional three-electrode electrochemical setup connected to a computer-controlled electrochemistry potentiostat was used under solar simulator irradiation. A platinum plate, an Ag/AgCl electrode, and TiO₂ or AgCl@TiO₂ thin film deposited on the woven wire mesh were utilized as the auxiliary, reference, and work electrodes, respectively. The measured potential vs that of the reversible hydrogen electrode (RHE) was calculated with the Nernst equation:

$$E_{RHE} = E_{Ag/AgCl} + 0.197\text{ V} + 0.059 \times \text{pH} \quad (2)$$

The photoelectrocatalytic activity of the prepared thin film photoanodes was measured in 0.5 M Na₂SO₄ (pH 6.5). The potential was recorded from negative to positive potentials at a scan rate of 100 mV s⁻¹.

2.5. Instrumentation

The powder phases analysis was determined by means of a Bruker/D8 Advanced diffractometer at 2θ ranging from 10° to 80° by step of 0.04° with graphite monochromatic CuK α radiation ($\lambda = 1.541 \text{ \AA}$). FESEM electron microscope and EDX analysis by MIRA3 TESCAN were used respectively for performing morphology and elemental maps of nanomaterials. The scanning tunneling microscopy (STM) images were taken by STM SS1 with Pt/Ir STM tip, 1.7 nA constant current, and 0.23 V voltage. An Agilent photodiode-array spectrophotometer Model 8453 equipped with quartz cell of 1 cm path length was used to obtain the UV–vis absorbance spectra of photocatalysts. A Shimadzu RF-1501 spectrophotometer was used to take the photoluminescence (PL) spectra of the prepared photocatalysts. The zeta potential of the nanomaterials was determined by the Zeta sizer (Nano-ZS) Malvern instrument. To observe surface morphology and thickness of film Atomic force microscopy (AFM) (JPK-NanoWizard II) was used. The determination of the total organic carbon (TOC) was performed using a 139 TOC analyzer (TOC-5000 A, Shimadzu). The Mott–Schottky plots were measured using a three-electrode system at a preset frequency at scan rate of 10 mV s⁻¹ and frequency of 500 Hz in 0.5 M Na₂SO₄ aqueous solution (pH = 6) by PG AUTOLAB model 302 N photoelectrochemical device. The fabrication of work electrode was conducted using spin coating of photocatalyst on the FTO.

3. Results and discussion

Powder XRD measurements were employed for confirmation of crystalline structures of the prepared photocatalysts. In Fig. 1, the XRD patterns of TiO₂ and AgCl@TiO₂ nanomaterials with different AgCl content (1, 3, 5, and 7%) are shown. The diffraction peaks of TiO₂ NPs can be assigned to both anatase (major) and rutile (minor) phases. It is found that there are the known diffraction peaks in 25.3, 37.8, 38.6, 48.0, 54.0, 62.7, 70.2, and 76.0° which indexed as the (1 0 1), (0 0 4), (1 1 2), (2 0 0), (1 0 5), (2 0 4), (2 2 0), and (2 1 5) crystal faces of TiO₂ anatase phase, respectively (Mu'izayanti and Sutrisno, 2018; Sangchay et al., 2012). Furthermore, it can be noticed that there are lower peaks in 27.2, 35.7, 40.9, 43.7, 56.1, and 68.3° that matched with the (1 1 0), (1 0 1), (1 1 1), (2 1 0), (2 2 0), and (3 0 1) of TiO₂ rutile crystal faces,

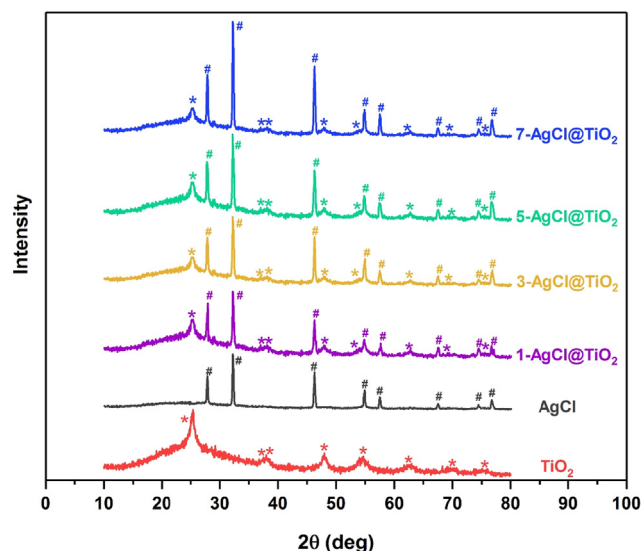


Fig. 1. XRD patterns of TiO₂ (anatase peaks were shown) and AgCl@TiO₂ (cubic AgCl peaks were shown) photocatalysts.

respectively (Mu'izayanti and Sutrisno, 2018). The XRD pattern of AgCl@TiO₂ sample contains the peaks of TiO₂ NPs as well as AgCl. The apparent diffraction peaks in 27.8, 32.2, 46.2, 54.8, 57.4, 67.4, 74.4, and 76.7° were rightly matched with the (1 1 1), (2 0 0), (2 2 0), (3 1 1), (2 2 2), (4 0 0), (3 3 1), and (4 2 0) reflections of a cubic crystal phase of AgCl (PDF file No. 01-085-1355) (Cao et al., 2011; Mu'izayanti and Sutrisno, 2018; Sangchay et al., 2012). The absence of any extra diffraction peaks in the XRD patterns of photocatalyst certifies samples' high level of purity (Karimi-Nazarabad et al., 2016). Moreover, the diffraction peaks of AgCl over AgCl@TiO₂ samples were slowly become stronger as the AgCl content increased.

The morphological properties of the electrodeposited photocatalysis substrates were investigated by means of the FESEM techniques. Fig. 2 shows FESEM images of TiO₂ and AgCl@TiO₂ photocatalysts and also elemental mapping of AgCl@TiO₂ thin film on the stainless steel mesh substrate. As it is evident from this figure, doping of AgCl has not influence on the structure and morphology of TiO₂ NPs. The elemental mapping analysis of AgCl@TiO₂ thin film on the stainless steel mesh substrate was shown in Fig. S1. It vividly shows the homogenous distribution of titanium, oxygen, chlorine, and silver. The EDX analysis demonstrates the AgCl content percentage in AgCl@TiO₂ samples which is 0.89, 2.76, 4.82, and 6.69% for 1-AgCl@TiO₂, 3-AgCl@TiO₂, 5-AgCl@TiO₂, and 7-AgCl@TiO₂, respectively. The nomination of AgCl@TiO₂ samples was done on this basis. The results further confirm that the AgCl is incorporated in the TiO₂ structure, which is in good agreement with the XRD. For determining the surface roughness, STM analysis of TiO₂ and AgCl@TiO₂ thin film on the stainless steel mesh was employed (Fig. S2). It demonstrates the surface topography of TiO₂ and AgCl@TiO₂ consisting of a series of black and bright clusters with the height of 12.4 and 11.3 nm, respectively.

The photoabsorption capability of the prepared photocatalysts was evaluated by the UV–vis spectroscopy, which is shown in Fig. 3a. The UV–vis spectra of 5-AgCl@TiO₂ and 7-AgCl@TiO₂ photocatalysts extend to the visible region in contrast to the pristine TiO₂ and 3-AgCl@TiO₂ photocatalyst. Higher capability for visible-light absorption by 5-AgCl@TiO₂ and 7-AgCl@TiO₂ photocatalysts leads to a better photocatalytic activity in comparison to the pristine TiO₂. Higher rates of harvesting visible light leads to an enhanced photo-generation charge carriers and therefore a superior photocatalytic activity would be achieved (Ong et al., 2016). This red shift, especially for 5-AgCl@TiO₂ photocatalyst, is due to the positive synergistic effect between AgCl and TiO₂ (Karimi-Nazarabad and Goharshadi, 2017). Due

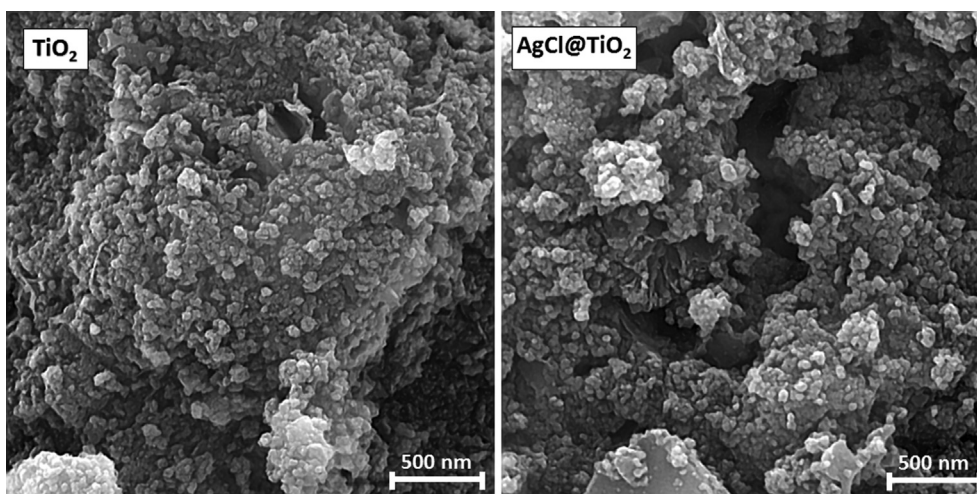


Fig. 2. FESEM images of TiO₂ and 5-AgCl@TiO₂ photocatalysts.

to the high content of AgCl in 7-AgCl@TiO₂, Fig. 3a shows characteristic absorption of AgCl in the range of 200–400 nm, in which the two peaks about 220 and 290 nm should be attributed to the direct and indirect exciton transitions of AgCl, respectively (Dong et al., 2013; Tian et al., 2014).

The predictable value of the band gap (E_g) of the photocatalysts could be calculated using Tauc equation (Ghanbari et al., 2017):

$$\alpha h\nu = A(h\nu - E_g)^{n/2} \quad (3)$$

where h , α , A , and ν are Planck's constant, absorption coefficient, a constant, and light frequency, respectively. The n values of 1 and 2 can be attributed to direct and indirect transitions, respectively. The value of 1 was assigned to TiO₂ and AgCl@TiO₂ nanomaterials (Yin et al., 2016). The evaluated values of E_g including 3.30, 3.42, 2.79, and 2.98 were assigned to the TiO₂, 3-AgCl@TiO₂, 5-AgCl@TiO₂, and 7-AgCl@TiO₂, respectively (Fig. 3b). Consequently, the value of energy band gap for 5-AgCl@TiO₂ photocatalyst illustrates a significant reduction which in turn, improves the visible light absorption ability and the photocatalytic performance of TiO₂.

PL spectroscopy can be considered as an applicable tool to assess the charge carrier's efficiency which is related to a number of factors including trapping, migration, and transfer, and also comprehending the charge carrier lifetime in semiconductor since PL emissions result from the recombination of free photo-generated charge carriers (Karimi-Nazarabad et al., 2019; Lim et al., 2015). The PL spectra of prepared photocatalysts are shown in Fig. 3c. Strength factor aside, the PL spectra for the four samples are almost identical. Due to the fast recombination of the photo-induced charge carriers, the higher PL intensity was attributed to TiO₂. The PL intensity of 5-AgCl@TiO₂ demonstrates a meaningful decrease compared with that of the other semiconductors. It indicated that the incorporation of AgCl in the structure of TiO₂ decreases the electron-hole recombination process. Therefore, since the 5-AgCl@TiO₂ photocatalyst possesses a longer carrier lifetime, a decrease in the PL intensity was observed, thereby photo-generated electron-hole pair separation is justified. Therefore, it is an important reason for the excellent photocatalytic performance of the hard-degradable methamphetamine removal. This can be attributed to the creation of a Schottky barrier at the Ag and TiO₂ interface, which could act as an electron sink to impressively halt the electron-hole recombination process (Lim et al., 2015). The lower PL intensity for 5-AgCl@TiO₂ in relation to TiO₂, demonstrates its superior separation capacity instigated by an interaction among AgCl and TiO₂. Furthermore, an additional peak of TiO₂ (at about 430 nm), belongs to the self-trapped excitons of TiO₆ octahedral would be observed (Klaysri et al., 2017).

The photodegradation of methamphetamine was investigated on the thin film stainless steel mesh substrates as photocatalysis under solar light irradiation. The solar light-responsive photocatalytic activity of methamphetamine degradation was observed for all of the AgCl doped TiO₂, as shown in Fig. 4. As shown in this figure, no photocatalytic degradation was observed for pure AgCl. The photocatalytic performance of AgCl@TiO₂ thin film was further enhanced by loading AgCl. The results show no photocatalytic degradation enhancement of methamphetamine in low AgCl doped (1%), indicating that the high AgCl doped percent was required. With further increasing the amount of AgCl from 1 to 5%, the photocatalytic degradation is increases quickly, and the performance achieves a maximum level when the amount of AgCl is about 5%. The enhancement of the photocatalytic efficiency of AgCl@TiO₂ thin film than TiO₂, is ascribed mainly to the effective separation of photo-generated electron-hole pairs which it was supported by comparing the PL spectra of TiO₂ and AgCl@TiO₂ photocatalysts (Fig. 3c). However, with a further increase in doped AgCl, a subsequent decrease of the photocatalytic degradation was observed. Overloading AgCl leads to growth and agglomeration of AgCl NPs in the TiO₂ structure, and some active sites of the TiO₂ structure could be shielded.

The flat band potentials of semiconductor photocatalyst can be attained from the x-axis intercept of the linear part fitted to the Mott-Schottky plot. Below Mott-Schottky equation is presented:

$$\frac{1}{C^2} = \left[\frac{2}{e_0 \epsilon_0 N_d} \right] \left[(V - V_{fb}) - \frac{k_B T}{e_0} \right] \quad (4)$$

where C is the specific capacitance (F cm⁻²), e_0 is the electron charge (1.602×10^{-19} C), ϵ is the semiconductor dielectric constant (18.9 for TiO₂ (Wypych et al., 2014)), ϵ_0 is the vacuum permittivity (8.854×10^{-14} F cm⁻¹), N_d is the carrier density, V is the electrode applied potential, k_B is Boltzmann constant, V_{fb} is the flat band potential, and T is the absolute temperature. In Fig. 5 the Mott-Schottky plots of the TiO₂ and 5-AgCl@TiO₂ is shown. The 0.15 and 0.05 were evaluated as flat band potential values for TiO₂ and 5-AgCl@TiO₂, respectively. Since the semiconductors are n-type, the slope of the Mott-Schottky plots are positive (Jiang et al., 2013; Karimi-Nazarabad et al., 2019). A more negative shift can be observed for AgCl@TiO₂ than TiO₂. Therefore, there is a greater carrier concentration in the hetero junction and more effectual charge transfer for AgCl@TiO₂ compared with TiO₂ (Liu et al., 2014).

Generally, the V_{fb} of a semiconductor corresponds to its Fermi level (EF) and is located under the conduction band (CB) edge for n-type semiconductors. The CB edge could be specified by V_{fb} . The equation given below can be used to calculate the CB energy level (when Ag/AgCl electrode is the reference) (Li et al., 2006; Mahvelati-Shamsabadi

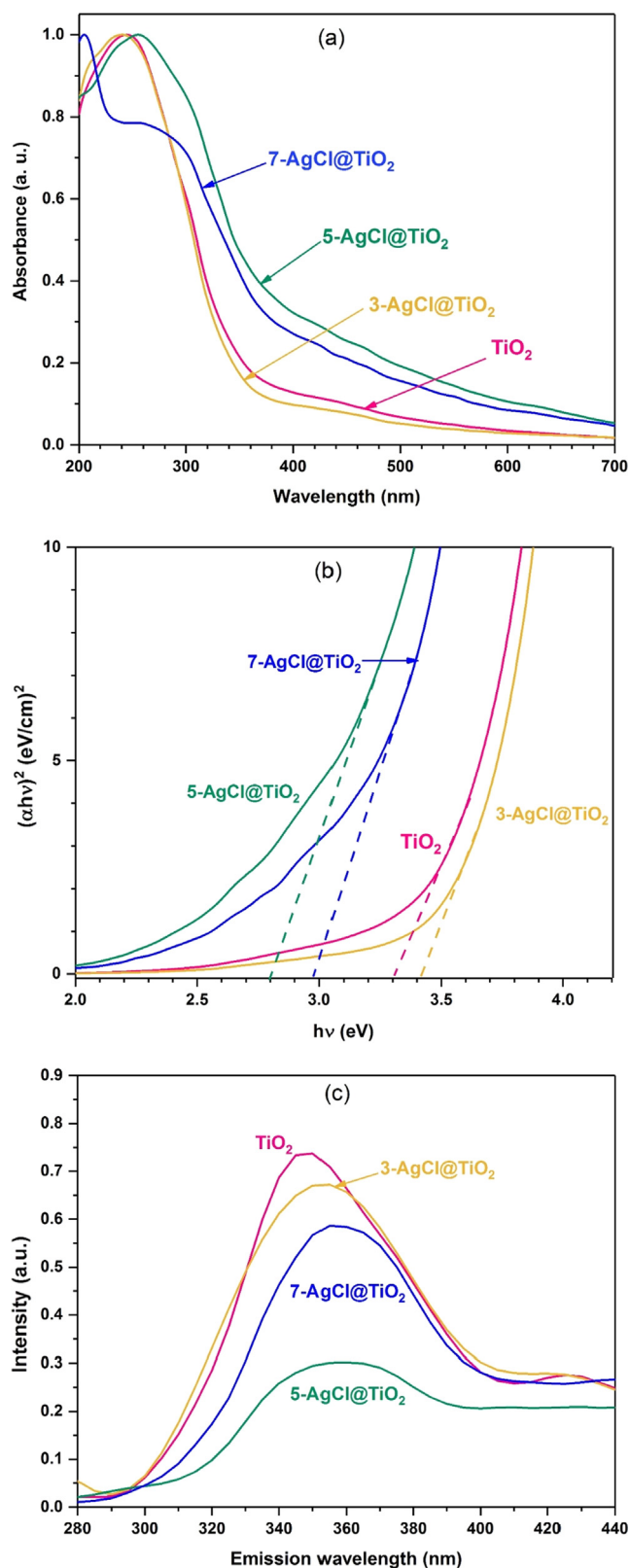


Fig. 3. (a) UV-vis spectrum, (b) Tauc plot, and (c) PL spectra of TiO₂ and different AgCl@TiO₂ photocatalysts dispersed in H₂O.

et al., 2019):

$$E_{CB} = -e(4.71 + V_{fb}) \quad (5)$$

where e stands for the reduced electron charge which is equal to 1. The

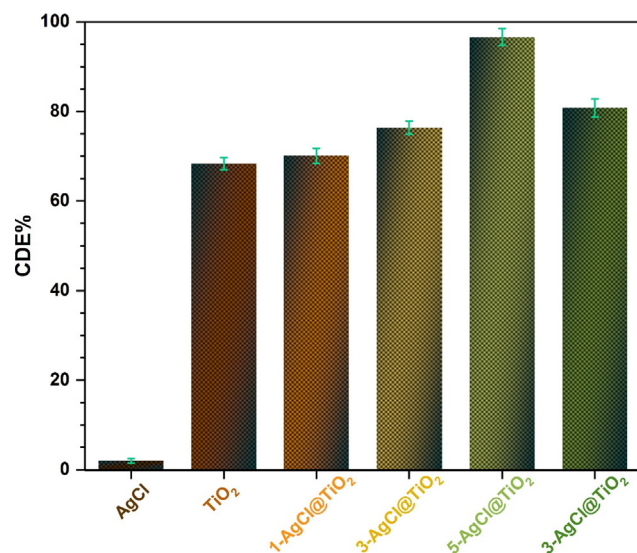


Fig. 4. Methamphetamine photodegradation in the presence of AgCl@TiO₂ with the different percentage of AgCl (pH = 7, t = 120 min, C₀ = 20 mg L⁻¹).

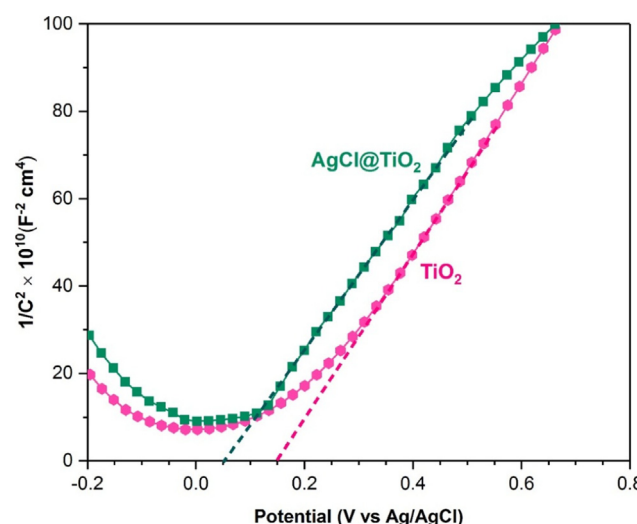


Fig. 5. Mott-Schottky plots of TiO₂ and 5-AgCl@TiO₂ electrodes at frequency of 500 Hz and scan rate of 10 mV s⁻¹.

$E_{VB} = E_{CB} - E_g$ relation can be assigned as valence band edge potential (E_{VB}). Fig. 6 exhibits the band diagrams of TiO₂ and 5-AgCl@TiO₂ photocatalysts. As it can be seen from band diagrams of semi-conductors, the CB of AgCl@TiO₂ has the appropriate situation to produce superoxide radicals for the photodegradation. On the other, the less band gap energy value for AgCl@TiO₂ increases solar light harvesting efficiency. Hence, the AgCl loading could significantly enhance the photo-generated charge carriers which lead to a greater photocatalytic degradation.

The electrostatic properties of the photocatalyst and the pollutant molecules were affected by solution pH. To evaluate the pH effect on ionization state of the photocatalyst surface, zeta potential variations were characterized as a function of different pH. The results of zeta potential analysis are shown in Fig. S4. The zero point charge (ZPC) for TiO₂ and 5-AgCl@TiO₂ was identified at pH = 3.3 and 4.1, respectively. At pH above pH_{zpc} , the zeta potential is negative showing that the surface charge of NPs is negative. The positive values for zeta potential observed in high acidic suspension at a pH lower than pH_{zpc} (Goharshadi et al., 2013; Azizi-Toupkanloo, et al., 2019). On the other, the dissociation constant (pK_a) of methamphetamine is 10.1 (Pavlova

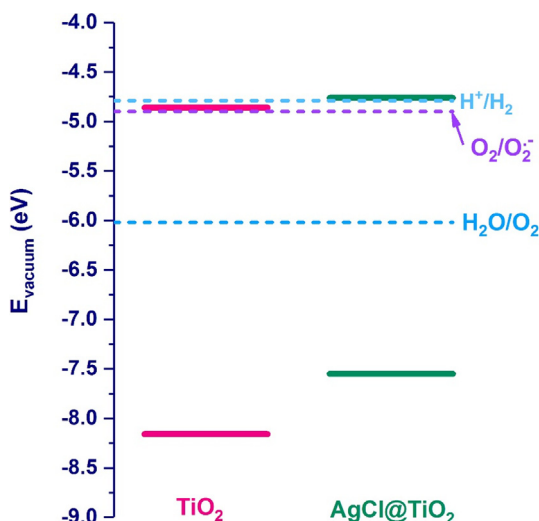


Fig. 6. The scheme of energy bands diagram of TiO₂ and 5-AgCl@TiO₂ semiconductors.

Table 1
The calculated anodic electrodeposited film thickness and mass of photocatalyst on the stainless steel mesh.

| <i>t</i> (s) | <i>d</i> (nm) |
|--------------|---------------|
| 0 | 0.0 |
| 30 | 162.9 |
| 60 | 325.7 |
| 120 | 651.5 |
| 180 | 977.2 |
| 240 | 1302.9 |
| 300 | 1628.7 |
| 360 | 1954.4 |

electrophoretic mobility ($\text{m}^2 \text{V}^{-1} \text{s}^{-1}$), *E* is the electric field (V m^{-1}), *C* is the particle mass concentration (mg m^{-3}), and *t* is the deposition time (s). For calculating the electrophoretic mobility, the Smoluchowski's mobility equation was used (Makino and Ohshima, 2010):

$$\mu = \frac{\epsilon_r \epsilon_0 \zeta}{\eta} \quad (8)$$

where ϵ_r is the relative permittivity (for TiO₂ is 18.9), η is the electrolyte solution viscosity ($0.000316 \text{ N s m}^{-2}$ for acetone), ϵ_0 is the permittivity of a vacuum ($8.854 \times 10^{-12} \text{ F m}^{-1}$), and ζ is the zeta potential. The electrophoretic mobility was obtained as $1.32 \times 10^{-8} \text{ m}^2 \text{V}^{-1} \text{s}^{-1}$. It has been found that by increasing time, deposition weight increased linearly. In Table 1 the effects of the time parameter on the film thickness of the photocatalysts is shown. From this table, we can conclude that as time increases, the electrodeposited photocatalyst mass increases as well and, at a constant loading concentration, leads to increase of the film thickness. The surface morphology and thickness of bare stainless steel mesh and AgCl@TiO₂ electrodeposited thin film for 300 s EPD were shown in Fig. S3. The thickness of photocatalyst film is 1480 nm which found to be in a reasonable agreement with the data in Table 1. This figure shows high surface roughness of the electrodeposited film which indicates growing branches from the depth of the deposited layer on the substrate.

Fig. 8 shows that increasing the film thickness of electrodeposited photocatalyst, as a significant parameter in the immobilized photocatalyst process, increases the efficiency of photocatalytic degradation. Enhancement of the photocatalytic degradation was continued until certain film thickness of photocatalyst is achieved and then no further

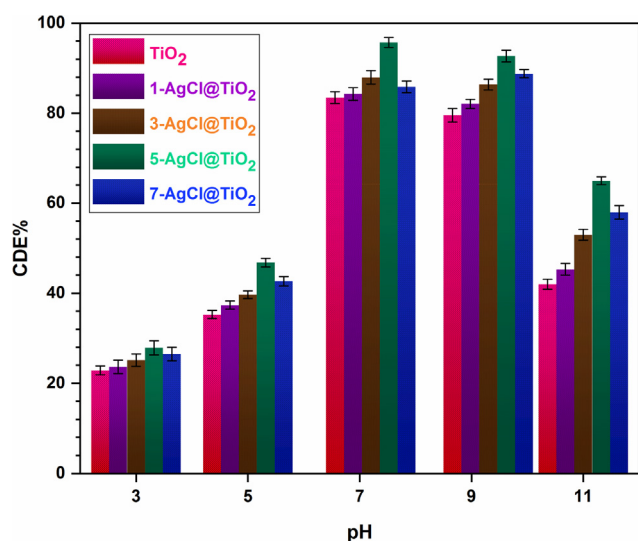


Fig. 7. Degradation of methamphetamine at different initial pH values for TiO₂ and AgCl@TiO₂ photocatalysts (*C*₀ = 20 mg L⁻¹, *t* = 120 min).

and Petrovska-Jovanovic, 2007), and hence, it is predicted that at pH values of about 4 to 10, methamphetamine adsorption can be completed on the photocatalyst surface. Fig. 7 shows the pH factor on the methamphetamine photodegradation for different initial pHs between 3 and 11. The maximum photodegradation was performed at the pHs of 7 and 9, which was predictable. Also, in all of the initial pHs the photodegradation by 5-AgCl@TiO₂ thin film is greater than other photocatalysts.

The film thickness was evaluated under applied electrodeposited time in the range of 0–360 s by the following equation:

$$d = \frac{m}{A\rho} \quad (6)$$

where ρ , *m*, *A*, and *d* are the density of TiO₂ (3.9 g cm^{-3}), deposition mass, surface area (4 cm^2), and thickness of photocatalyst film, respectively. The anodic electrodeposited mass of the photocatalyst was calculated by Hamaker's equation (Collini et al., 2017; Fang et al., 2015):

$$m(t) = f\mu CAEt \quad (7)$$

where *f* is the efficiency of the process (assuming *f* = 1), μ is the

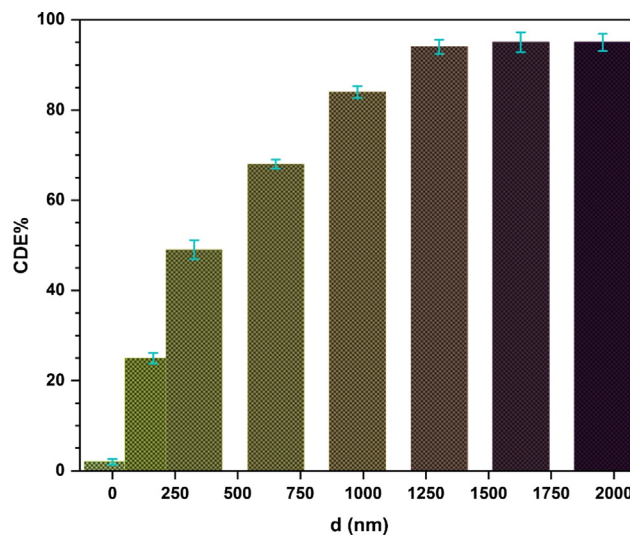


Fig. 8. Photodegradation efficiency of methamphetamine by 5-AgCl@TiO₂ film with different film thickness of the photocatalyst (pH = 7, *t* = 120 min, *C*₀ = 20 mg L⁻¹).

Table 2
The catalytic performance comparison of different systems for methamphetamine degradation.

| Catalyst | Amount of catalyst (g L ⁻¹) | Concentration of methamphetamine (mg L ⁻¹) | Energy source | Degradation efficiency (%) | Ref. |
|--|---|--|---------------|----------------------------|----------------------|
| ZnO | 0.01–1 | 0.1 | UV lamp | 100 | (Lin et al., 2013) |
| Degussa P25 | 0.01–1 | 0.1 | UV LED | 100 | (Lin et al., 2013) |
| Degussa P25 | 0.1 | 10 | UV lamp | 100 | (Kuo et al., 2015) |
| Er ³⁺ :YAlO ₃ /Nb ₂ O ₅ | 1.0 | 10 | Ultrasound | 82 | (Wei et al., 2018) |
| Er ³⁺ :Y ₃ Al ₅ O ₁₂ /WO ₃ -KNbO ₃ | 1.0 | 10 | Ultrasound | 68 | (Zhang et al., 2017) |
| AgCl@TiO ₂ film | 0.085 | 20 | Solar light | 100 | Present work |

changes would happen. The optimal efficiency of photodegradation was attained in the film thickness of 1629 nm. It seems that the surface of the stainless steel mesh as a substrate was completely coated by photocatalyst within 300 s from the onset of the electrodeposition time. Actually, as the film thickness increases, the enhancing of the active sites on the surface of photocatalyst thin film was observed and, therefore, more radical species will be produced. Besides, it causes the film resistance to increase, hence the electron transport routes are prolonged and recombination of photo-generated charge carrier are enhanced (Zargazi and Entezari, 2019).

The photocatalysts are commonly employed as powder. In the aqueous dispersion, there are some difficulties such as low photodegradation efficiency and low recovery of the photocatalyst which poses some significant restrictions on their application. In order to overcome the problems, deposited photocatalyst was immobilized on the desired green substrate which shows excellent photocatalytic performance in comparison with powders. The degradation of methamphetamine by reported different catalysts and present fabricated AgCl@TiO₂ film was compared as shown in Table 2. The AgCl@TiO₂ film with a smaller amount of catalyst was able to degrade a higher concentration of methamphetamine in the presence of natural solar light.

For scale up photocatalytic degradation, reusability, durability, and endurance of photocatalyst films are considered as significant parameters (Li et al., 2016). For a long period of time, a cost-effective photocatalyst performance should not be decreased (Adamek et al., 2019). To study these issues, the degradation of methamphetamine was repeated ten successive cycles using different photocatalysts thin films, as shown in Fig. 9. During each cycle, the washing and drying of thin film was applied, and reused in fresh methamphetamine solution while being exposed to solar light irradiation. The photocatalysts thin films are capable of removing hard-degradable methamphetamine at any

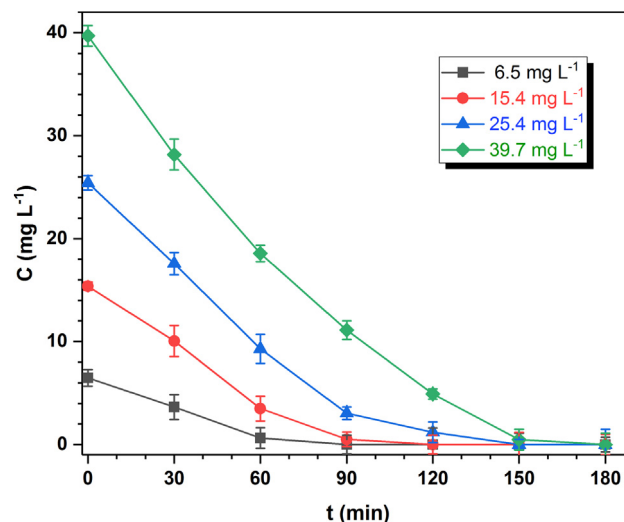


Fig. 10. The photocatalytic degradation of methamphetamine by 5-AgCl@TiO₂ under solar light irradiation at pH = 7.

time without any significant reduction of efficiency. Therefore, the photocatalysts are neither destroyed nor separated from the substrate surface. It shows that photocatalysts thin films were stable in the presence of solar light irradiation and TiO₂ or AgCl@TiO₂ attached powerfully on the stainless steel mesh. Hence, the photocatalyst thin film has the high-performance for hard-degradable contaminants and could be utilized for high-scale photodegradation. Most photodegradation efficiency was observed for 5-AgCl@TiO₂.

As indicated in Fig. 10, the photodegradation of methamphetamine was evaluated in the 6–40 mg L⁻¹ range of concentration, in the presence of solar light. The photodegradation time was increased when the methamphetamine concentration increases. The longer degradation time is ascribed to the decrease of the active sites on the photocatalysts surface and the amount of produced radical species versus the number of methamphetamine molecules. Therefore, the initial concentration of pollutant can be found as one of the important factors on the photocatalytic performance of photocatalyst thin film.

In order to determine the level of mineralization, TOC of methamphetamine and photodegraded sample by TiO₂ and AgCl@TiO₂ thin films were measured after being irradiated in the presence of solar light for 180 min. Fig. 11 shows the residual ratio TOC/TOC₀ for photodegradation of methamphetamine. The TOC/TOC₀ value is lower for 5-AgCl@TiO₂ thin film compared to other thin films. This implies that, the mineralization of methamphetamine by 5-AgCl@TiO₂ thin film is about 91%. Consequently, these results suggest that the doping of AgCl in the TiO₂ NPs facilitate the separation of holes and electrons, thereby increasing the TOC degradation under solar irradiation. It could be concluded that methamphetamine could be completely degraded with less residues of transformation products formed during the photocatalytic process.

The photoelectrochemical performance of TiO₂ and AgCl@TiO₂ thin film deposited on the woven wire mesh as photoanodes was considered by means of the LSV technique under solar simulator irradiation

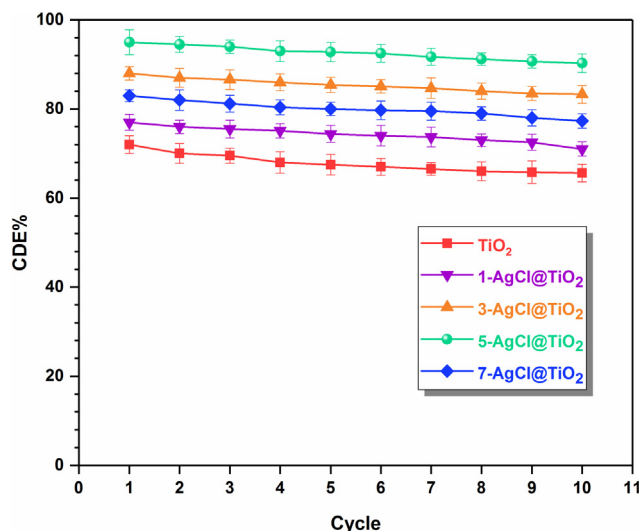


Fig. 9. The reusability of TiO₂ and AgCl@TiO₂ photocatalysts in consecutive cycles (pH = 7, t = 120 min, C₀ = 20 mg L⁻¹).

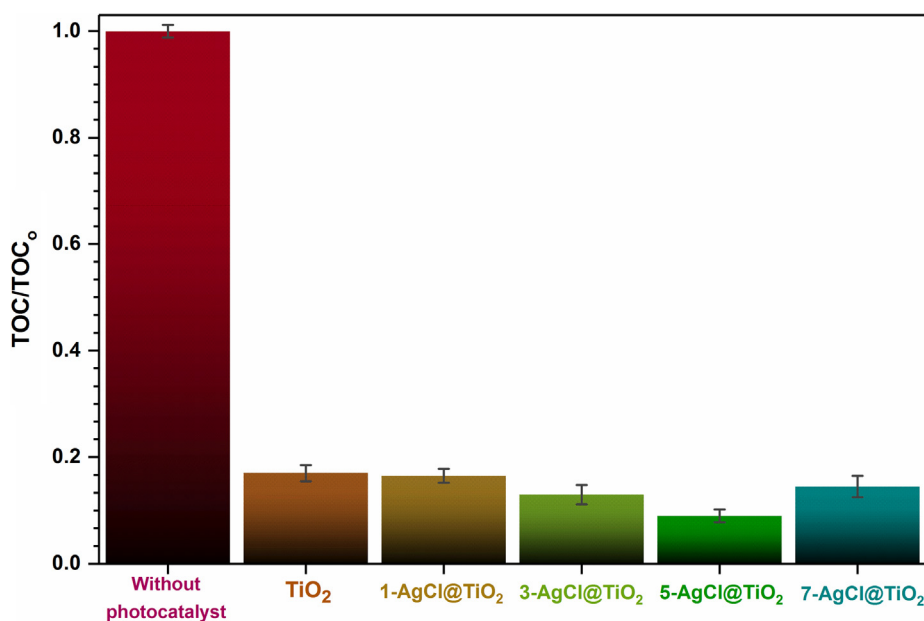


Fig. 11. The residual ratio TOC/TOC_0 for photodegradation of methamphetamine by TiO_2 and $5-AgCl@TiO_2$ photocatalysts (pH = 7, $t = 180$ min, $C_0 = 20$ mg L⁻¹).

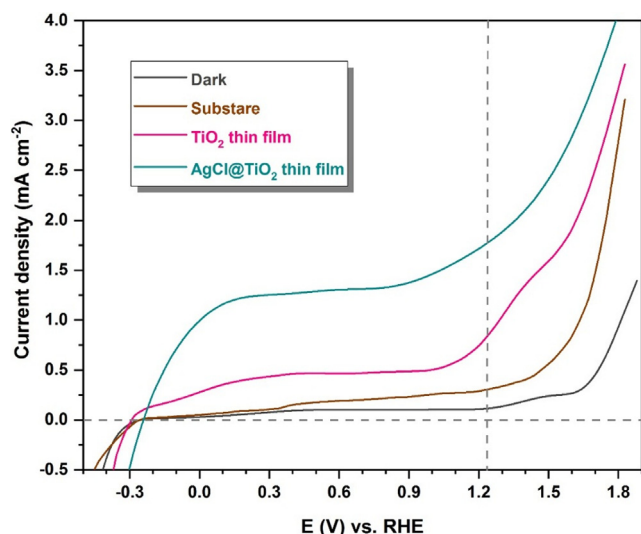


Fig. 12. Current density vs potential for substrate (woven wire mesh), TiO_2 , and $5-AgCl@TiO_2$ photoelectrodes. The vertical dashed line indicates the potential of oxygen evolution reaction vs RHE.

(Fig. 12). The higher photocurrent density supplies a strong driving force for the photoelectrochemical device in the water splitting process (Karimi-Nazarabad et al., 2019). The small current density was observed for all thin film photoanodes in the dark. According to the TiO_2 thin film electrode results, a photocurrent density of 0.85 mA cm⁻² at 1.23 V vs RHE corresponding to oxygen evolution reaction were achieved. After incorporation of AgCl in the TiO_2 structure, the photocurrent density significantly enhanced to 1.8 mA cm⁻² demonstrating that the photoelectrocatalytic performance of TiO_2 toward the oxygen evolution reaction has improved.

4. Conclusions

$AgCl@TiO_2$ electrodeposited thin film on woven wire mesh was presented as an efficient treatment configuration for removing hard-degradable methamphetamine from the water under natural solar light. Among the prepared photocatalysts, the $5-AgCl@TiO_2$ had the highest

photocatalytic activity in degradation of methamphetamine. The Mott-Schottky plots analysis demonstrates a greater carrier concentration in the hetero junction and hence more effectual charge transfer for $AgCl@TiO_2$ compared with TiO_2 . Film thickness and pH were two factors affecting photodegradation process the most. A film thickness of 1629 nm yields the optimal photocatalytic activity. Additionally, after ten consecutive cycles, the durability and stability of thin film has not been changed in photocatalytic process. It is worth noting that; a rather more complete mineralization (> 90%) of methamphetamine was obtained with $5-AgCl@TiO_2$ photocatalysis substrate after 180 min. A photocurrent density of 1.8 mA cm⁻² at 1.23 V vs RHE corresponding to oxygen evolution reaction were achieved for $5-AgCl@TiO_2$.

Acknowledgement

The authors express their gratitude to University of Neyshabur for financial support of this project (Grant No. 97/15432).

Declaration of Competing Interest

The authors declare that there is no conflict of interest regarding the publication of this article.

Appendix A. Supplementary material

Supplementary data to this article can be found online at <https://doi.org/10.1016/j.solener.2019.12.046>.

References

- Adamek, E., Baran, W., Ziemiańska-Błaszczak, J., Sobczak, A., 2019. Immobilisation of TiO_2 -P25 on a glass fibre mat: preparation, photocatalytic activity and stability. *Sol. Energy* 188, 1232–1242. <https://doi.org/10.1016/j.solener.2019.07.034>.
- Anitha, V.C., Banerjee, A.N., Joo, S.W., 2015. Recent developments in TiO_2 as n- and p-type transparent semiconductors: synthesis, modification, properties, and energy-related applications. *J. Mater. Sci.* 50, 7495–7536. <https://doi.org/10.1007/s10853-015-9303-7>.
- Bagnall, J., Malia, L., Lubben, A., Kasprzyk-Hordern, B., 2013. Stereoselective biodegradation of amphetamine and methamphetamine in river microcosms. *Water Res.* 47, 5708–5718. <https://doi.org/10.1016/j.watres.2013.06.057>.
- Brindha, A., Sivakumar, T., 2017. Visible active N, S co-doped TiO_2 /graphene photocatalysts for the degradation of hazardous dyes. *J. Photochem. Photobiol. A Chem.* 340, 146–156. <https://doi.org/10.1016/j.jphotochem.2017.03.010>.

- Cao, J., Xu, B., Luo, B., Lin, H., Chen, S., 2011. Preparation, characterization and visible-light photocatalytic activity of Ag/AgCl/TiO₂. *Appl. Surf. Sci.* 257, 7083–7089. <https://doi.org/10.1016/j.apsusc.2011.03.046>.
- Carbonaro, S., Sugihara, M.N., Strathmann, T.J., 2013. Continuous-flow photocatalytic treatment of pharmaceutical micropollutants: activity, inhibition, and deactivation of TiO₂ photocatalysts in wastewater effluent. *Appl. Catal. B Environ.* 129, 1–12. <https://doi.org/10.1016/j.apcatb.2012.09.014>.
- Castiglioni, S., Bagnati, R., Melis, M., Panawennage, D., Chiarelli, P., Fanelli, R., Zuccato, E., 2011. Identification of cocaine and its metabolites in urban wastewater and comparison with the human excretion profile in urine. *Water Res.* 45, 5141–5150. <https://doi.org/10.1016/j.watres.2011.07.017>.
- Chang, S., Yang, X., Sang, Y., Liu, H., 2016. Highly efficient photocatalysts and continuous-flow photocatalytic reactors for degradation of organic pollutants in wastewater. *Chem. - An Asian J.* 11, 2352–2371. <https://doi.org/10.1002/asia.201600363>.
- Collini, P., Kota, S., Dillon, A.D., Barsom, M.W., Fafarman, A.T., 2017. Electrophoretic deposition of two-dimensional titanium carbide (MXene) thick films. *J. Electrochem. Soc.* 164, D573–D580. <https://doi.org/10.1149/2.0211709jes>.
- Dong, R., Tian, B., Zeng, C., Li, T., Wang, T., Zhang, J., 2013. Ecofriendly synthesis and photocatalytic activity of uniform cubic Ag@AgCl plasmonic photocatalyst. *J. Phys. Chem. C* 117, 213–220. <https://doi.org/10.1021/jp311970k>.
- Elkoro, A., Soler, L., Llorca, J., Casanova, I., 2019. 3D printed microstructured Au/TiO₂ catalyst for hydrogen photoproduction. *Appl. Mater. Today* 16, 265–272. <https://doi.org/10.1016/j.apmt.2019.06.007>.
- Evgenidou, E.N., Konstantinou, I.K., Lambropoulou, D.A., 2015. Occurrence and removal of transformation products of PPCPs and illicit drugs in wastewaters: a review. *Sci. Total Environ.* 505, 905–926. <https://doi.org/10.1016/j.scitotenv.2014.10.021>.
- Fang, Y., Lee, W.C., Canciani, G.E., Draper, T.C., Al-Bawi, Z.F., Bedi, J.S., Perry, C.C., Chen, Q., 2015. Thickness control in electrophoretic deposition of WO₃ nanofiber thin films for solar water splitting. *Mater. Sci. Eng. B Solid-State Mater. Adv. Technol.* 202, 39–45. <https://doi.org/10.1016/j.mseb.2015.09.005>.
- Ganeshraya, A.S., Zhu, K., Nomura, K., Wang, J., 2018. Hierarchical assembly of AgCl@Sn-TiO₂ microspheres with enhanced visible light photocatalytic performance. *Appl. Surf. Sci.* 441, 678–687. <https://doi.org/10.1016/j.apsusc.2018.01.262>.
- Ghanbari, M., Rounaghi, G.H., Ashraf, N., Paydar, M., Razavipanah, I., Karimi-Nazarabad, M., 2017. A facile approach for synthesis of a novel WO₃-g-C₃N₄/Pt-Sn-Os catalyst and its application for methanol electro-oxidation. *J. Clust. Sci.* 28, 2133–2146. <https://doi.org/10.1007/s10876-017-1208-y>.
- Goharshadi, E.K., Hadadian, M., Mahdi, M., Azizi-Toupanloo, H., 2013. Photocatalytic degradation of reactive black 5 azo dye by zinc sulfide quantum dots prepared by a sonochemical method. *Mater. Sci. Semicond. Process.* 16 (16), 1109–1116. <https://doi.org/10.1016/j.mssp.2013.03.005>.
- Hao, Z., Li, Shuyuan, Sun, J., Li, Song, Zhang, F., 2018. Efficient visible-light-driven degradation of oxidized lignin to aromatics catalyzed by an iridium complex immobilized on mesocellular silica foams. *Appl. Catal. B Environ.* 237, 366–372. <https://doi.org/10.1016/j.apcatb.2018.05.072>.
- Hong, X., Tan, J., Zhu, H., Feng, N., Yang, Y., Irvine, J.T.S., Wang, L., Liu, G., Cheng, H.-M., 2019. Control of spatially homogeneous distribution of heteroatoms to produce red TiO₂ photocatalyst for visible-light photocatalytic water splitting. *Chem. - A Eur. J.* 25, 1787–1794. <https://doi.org/10.1002/chem.201805283>.
- Azizi-Toupanloo, H., Karimi-Nazarabad, M., Shakeri, M., Eftekhari, M., 2019. Photocatalytic mineralization of hard-degradable morphine by visible light-driven Ag@g-C₃N₄ nanosheets. *Environ. Sci. Pollut. Res.* 26, 30941–30953. <https://doi.org/10.1007/s11356-019-06274-9>.
- Huo, P., Yan, Y., Li, S., Li, H., Huang, W., 2010. Floating photocatalysts of fly-ash cenospheres supported AgCl/TiO₂ films with enhanced Rhodamine B photodecomposition activity. *Desalination* 256, 196–200. <https://doi.org/10.1016/j.desal.2010.01.012>.
- Jiang, T., Xie, T., Yang, W., Chen, L., Fan, H., Wang, D., 2013. Photoelectrochemical and photovoltaic properties of p-n Cu₂O homojunction films and their photocatalytic performance. *J. Phys. Chem. C* 117, 4619–4624.
- Jones, O.A.H., Voulvoulis, N., Lester, J.N., 2002. Aquatic environmental assessment of the top 25 English prescription pharmaceuticals. *Water Res.* 36, 5013–5022. [https://doi.org/10.1016/S0043-1354\(02\)00227-0](https://doi.org/10.1016/S0043-1354(02)00227-0).
- Karimi-Nazarabad, M., Goharshadi, E.K., 2017. Highly efficient photocatalytic and photoelectrocatalytic activity of solar light driven WO₃/g-C₃N₄ nanocomposite. *Sol. Energy Mater. Sol. Cells* 160, 484–493. <https://doi.org/10.1016/j.solmat.2016.11.005>.
- Karimi-Nazarabad, M., Goharshadi, E.K., Mahdizadeh, S.J., 2019. Efficient photoelectrocatalytic water oxidation by palladium doped g-C₃N₄ electrodeposited thin film. *J. Phys. Chem. C* 123 (43), 26106–26115. <https://doi.org/10.1021/acs.jpcc.9b07755>.
- Kasprzyk-Hordern, B., Dinsdale, R.M., Guwy, A.J., 2009. Illicit drugs and pharmaceuticals in the environment - Forensic applications of environmental data. Part 1: estimation of the usage of drugs in local communities. *Environ. Pollut.* 157, 1773–1777. <https://doi.org/10.1016/j.envpol.2009.03.017>.
- Kates, L.N., Knapp, C.W., Keenan, H.E., 2014. Acute and chronic environmental effects of clandestine methamphetamine waste. *Sci. Total Environ.* 493, 781–788. <https://doi.org/10.1016/j.scitotenv.2014.06.066>.
- Klaysri, R., Tubchareon, T., Prasertthad, P., 2017. One-step synthesis of amine-functionalized TiO₂ surface for photocatalytic decolorization under visible light irradiation. *J. Ind. Eng. Chem.* 45, 229–236. <https://doi.org/10.1016/j.jiec.2016.09.027>.
- Kuo, C.S., Lin, C.F., Hong, P.K.A., 2015. Photocatalytic degradation of methamphetamine by UV/TiO₂-Kinetics, intermediates, and products. *Water Res.* 74, 1–9. <https://doi.org/10.1016/j.watres.2015.01.043>.
- Li, X., Hao, Z., Zhang, F., Li, H., 2016. Reduced graphene oxide-immobilized tris(bipyridine)ruthenium(II) complex for efficient visible-light-driven reductive dehalogenation reaction. *ACS Appl. Mater. Interfaces* 8, 12141–12148. <https://doi.org/10.1021/acsami.6b01100>.
- Li, Y.C., Zhong, H.Z., Li, R., Zhou, Y., Yang, C.H., Li, Y.F., 2006. High-yield fabrication and electrochemical characterization of tetrapodal CdSe, CdTe, and CdSe₂Te_{1-x} nanocrystals. *Adv. Funct. Mater.* 16, 1705–1716.
- Lim, S.P., Pandikumar, A., Lim, H.N., Ramaraj, R., Huang, N.M., 2015. Boosting photochemical performance of dye-sensitized solar cells using silver nanoparticle-decorated N, S-Co-doped-TiO₂ photoanode. *Sci. Rep.* 5, 11922. <https://doi.org/10.1038/srep11922>.
- Lin, C.F., Shiu, Y.J., Kuo, C.S., Lin, A.Y.C., Wu, C.H., Andy Hong, P.K., 2013. Photocatalytic degradation of morphine, methamphetamine, and ketamine by illuminated TiO₂ and ZnO. *React. Kinet. Mech. Catal.* 110, 559–574. <https://doi.org/10.1007/s11144-013-0621-y>.
- Liu, Q., Lu, H., Shi, Z., Wu, F., Guo, J., Deng, K., Li, L., 2014. 2D ZnIn₂S₄ nanosheet/1D TiO₂ nanorod heterostructure arrays for improved photoelectrochemical water splitting. *ACS Appl. Mater. Interfaces* 6, 17200–17207. <https://doi.org/10.1021/am505015j>.
- Lv, X., Wang, T., Jiang, W., 2018. Preparation of Ag@AgCl/g-C₃N₄/TiO₂ porous ceramic films with enhanced photocatalysis performance and self-cleaning effect. *Ceram. Int.* 44, 9326–9337. <https://doi.org/10.1016/j.ceramint.2018.02.145>.
- Mahvelati-Shamsabadi, T., Goharshadi, E.K., Karimi-Nazarabad, M., 2019. Z-scheme design of Ag@g-C₃N₄/ZnS photoanode device for efficient solar water oxidation: an organic-inorganic electronic interface. *Int. J. Hydrogen Energy.* 44, 13085–13097. <https://doi.org/10.1016/j.ijhydene.2019.03.242>.
- Makino, K., Oshima, H., 2010. Electrophoretic mobility of a colloidal particle with constant surface charge density. *Langmuir* 26, 18016–18019. <https://doi.org/10.1021/la1035745>.
- Monga, A., Bathla, A., Pal, B., 2017. A Cu-Au bimetallic co-catalysis for the improved photocatalytic activity of TiO₂ under visible light irradiation. *Sol. Energy* 155, 1403–1410. <https://doi.org/10.1016/j.solener.2017.07.084>.
- Mu'izayanti, V.A., Sutrisno, H., 2018. Structural and optical properties of AgCl-sensitized TiO₂ (TiO₂@AgCl) prepared by a reflux technique under alkaline condition. *Ceramica* 64, 190–196. <https://doi.org/10.1590/0366-69132018643702311>.
- Ong, W.-J., Tan, L.-L., Ng, Y.H., Yong, S.-T., Chai, S.-P., 2016. Graphitic carbon nitride (g-C₃N₄)-based photocatalysts for artificial photosynthesis and environmental remediation: are we a step closer to achieving sustainability? *Chem. Rev.* 116, 7159–7329. <https://doi.org/10.1021/acs.chemrev.6b00075>.
- Pavlova, V., Petrovska-Jovanovic, S., 2007. Simultaneous determination of amphetamine, methamphetamine, and caffeine in seized tablets by high-performance liquid chromatography. *Acta Chromatogr.* 18, 157.
- Putri, L.K., Ong, W.-J., Chang, W.S., Chai, S.-P., 2016. Enhancement in the photocatalytic activity of carbon nitride through hybridization with light-sensitive AgCl for carbon dioxide reduction to methane. *Catal. Sci. Technol.* 6, 744–754. <https://doi.org/10.1039/c5cy00767d>.
- Rosa Boleda, M., Huerta-Fontela, M., Ventura, F., Galceran, M.T., 2011. Evaluation of the presence of drugs of abuse in tap waters. *Chemosphere* 84, 1601–1607. <https://doi.org/10.1016/j.chemosphere.2011.05.033>.
- Sangchay, W., Sikong, L., Kooptarnond, K., 2012. Comparison of photocatalytic reaction of commercial P25 and synthetic TiO₂-AgCl nanoparticles. *Procedia Eng. Elsevier Ltd* 590–596. <https://doi.org/10.1016/j.proeng.2012.01.1313>.
- Tayebi, M., Kolaei, M., Tayyebi, A., Masoumi, Z., Belbasi, Z., Lee, B.K., 2019. Reduced graphene oxide (RGO) on TiO₂ for an improved photoelectrochemical (PEC) and photocatalytic activity. *Sol. Energy* 190, 185–194. <https://doi.org/10.1016/j.solener.2019.08.020>.
- Ternes, T.A., 2001. Analytical methods for the determination of pharmaceuticals in aqueous environmental samples. *TrAC - Trends Anal. Chem.* 20, 419–434. [https://doi.org/10.1016/S0165-9936\(01\)00078-4](https://doi.org/10.1016/S0165-9936(01)00078-4).
- Tian, B., Dong, R., Zhang, J., Bao, S., Yang, F., Zhang, J., 2014. Sandwich-structured AgCl at Ag at TiO₂ with excellent visible-light photocatalytic activity for organic pollutant degradation and E. coli K12 inactivation. *Appl. Catal. B Environ.* 158–159, 76–84. <https://doi.org/10.1016/j.apcatb.2014.04.008>.
- Wang, P., Huang, B., Qin, X., Zhang, X., Dai, Y., Wei, J., Whangbo, M.-H., 2008. Ag@AgCl: a highly efficient and stable photocatalyst active under visible light. *Angew. Chemie Int. Ed.* 47, 7931–7933. <https://doi.org/10.1002/anie.200802483>.
- Wang, Z., Xu, Z., Li, X., 2018. Biodegradation of methamphetamine and ketamine in aquatic ecosystem and associated shift in bacterial community. *J. Hazard. Mater.* 359, 356–364. <https://doi.org/10.1016/j.jhazmat.2018.07.039>.
- Wei, C., Yi, K., Sun, G., Wang, J., 2018. Synthesis of novel sonocatalyst Er³⁺:YAlO₃/Nb₂O₅ and its application for sonocatalytic degradation of methamphetamine hydrochloride. *Ultrason. Sonochem.* 42, 57–67. <https://doi.org/10.1016/j.ultrsonch.2017.10.031>.
- Wypych, A., Bobowska, I., Tracz, M., Opasinska, A., Kadlubowski, S., Krzywaniak-Kaliszewska, A., Grobelny, J., Wojciechowski, P., 2014. Dielectric properties and characterisation of titanium dioxide obtained by different chemistry methods. *J. Nanomater.* 2014, 124814–124823. <https://doi.org/10.1155/2014/124814>.
- Yang, Q., Hu, M., Guo, J., Ge, Z., Feng, J., 2018. Synthesis and enhanced photocatalytic performance of Ag/AgCl/TiO₂ nanocomposites prepared by ion exchange method. *J. Mater.* 4, 402–411. <https://doi.org/10.1016/j.jmat.2018.06.002>.
- Yin, H., Wang, X., Wang, L., Nie, Q., Zhang, Y., Yuan, Q., Wu, W., 2016. Ag/AgCl modified self-doped TiO₂ hollow sphere with enhanced visible light photocatalytic activity. *J. Alloys Compd.* 657, 44–52. <https://doi.org/10.1016/j.jallcom.2015.10.055>.
- Yuan, W., Cheng, L., Zhang, Y., Wu, H., Lv, S., Chai, L., Guo, X., Zheng, L., 2017. 2D-layered carbon/TiO₂ hybrids derived from Ti₃C₂MXenes for photocatalytic hydrogen

- evolution under visible light irradiation. *Adv. Mater. Interfaces* 4, 1700577. <https://doi.org/10.1002/admi.201700577>.
- Zargazi, M., Entezari, M.H., 2019. Anodic electrophoretic deposition of Bi₂WO₆ thin film: high photocatalytic activity for degradation of a binary mixture. *Appl. Catal. B Environ.* 242, 507–517. <https://doi.org/10.1016/j.apcatb.2018.09.093>.
- Zhang, H., Huang, Y., Li, G., Wang, G., Fang, D., Song, Y., Wang, J., 2017. Preparation of Er³⁺:Y₃Al₅O₁₂/WO₃-KNbO₃ composite and application in treatment of methamphetamine under ultrasonic irradiation. *Ultrason. Sonochem.* 35, 478–488. <https://doi.org/10.1016/j.ultsonch.2016.11.004>.